

# Solovay Kitaev and Randomized Compilation

Oliver Maupin,<sup>1</sup> Ashlyn D. Burch,<sup>2,\*</sup> Christopher G. Yale,<sup>2</sup> Matthew N. H. Chow,<sup>2,3,†</sup> Terra Colvin, Jr.,<sup>4</sup> Brandon Ruzic,<sup>2</sup> Melissa C. Revelle,<sup>2</sup> Brian K. McFarland,<sup>2</sup> Eduardo Ibarra-García-Padilla,<sup>2</sup> Alejandro Rascon,<sup>2,3</sup> Andrew J. Landahl,<sup>2,3</sup> Susan M. Clark,<sup>2</sup> and Peter J. Love<sup>4,5</sup>

<sup>1</sup>*Quantum Performance Laboratory, Sandia National Laboratories, Albuquerque, NM, 87185, and Livermore, CA, 94550, USA*

<sup>2</sup>*Sandia National Laboratories, Albuquerque, NM, 87185, USA*

<sup>3</sup>*Department of Physics and Astronomy, University of New Mexico, Albuquerque, NM, 87131, USA*

<sup>4</sup>*Department of Physics and Astronomy, Tufts University, Medford, MA, 02155, USA*

<sup>5</sup>*Computational Science Initiative, Brookhaven National Laboratory, Upton, NY, 11973, USA*

We analyze the use of the Solovay Kitaev (SK) algorithm to generate an ensemble of one qubit rotations over which to perform randomized compilation. We perform simulations to compare the trace distance between the quantum state resulting from an ideal one qubit  $R_Z$  rotation and discrete SK decompositions. We find that this simple randomized gate synthesis algorithm can reduce the approximation error of these rotations in the absence of quantum noise by at least a factor of two. We test the technique under the effects of a simple coherent noise model and find that it can mitigate coherent noise. We also run our algorithm on Sandia National Laboratories' QSCOUT trapped-ion device and find that randomization is able to help in the presence of realistic noise sources.

## I. INTRODUCTION

Quantum computing is currently in the Noisy Intermediate Scale Quantum (NISQ) era of development [1]. NISQ computers exhibit quantum coherence, scale to hundreds of qubits, achieve error rates of less than 1%, and have enabled many small-scale demonstrations of quantum algorithms, as well as larger scale “quantum supremacy” experiments [2]. NISQ machines lack quantum error correction, however a wide range of error mitigation techniques have been developed which aim to extract better results from noisy quantum data [3].

To move beyond the NISQ era requires implementation of quantum error correction (QEC) [4]. QEC encodes each logical qubit in many physical qubits. If the error rate on the physical qubits is below a threshold (whose value depends on the particular scheme used) then the error rates for all encoded gates on the logical qubits can be lower than those on the physical qubits. This enables continued reduction in error rates at the price of more physical qubits, but without further improvements in physical qubit noise. These techniques are necessary to reach the very large numbers of qubits and gate operations that are required by applications at the quantum advantage scale.

With recent demonstrations of logical qubits in several platforms we are seeing the first demonstrations of post-NISQ quantum technology [5–8]. This new era of development has been termed Early Fault Tolerant Quantum Computation (EFTQC) [9]. Like NISQ, these EFTQC demonstrations will inform the development of future large scale quantum computation. These advancements

raise the question of whether NISQ experiments can inform the development of EFTQC devices? In the present paper we address one aspect of this question by considering a key element of QEC, the decomposition of continuous operations into circuits over a discrete gate set.

For ion trap systems the physical single-qubit gates are significantly better than the two-qubit gates. This can pose a challenge to demonstrations of QEC as the encoded one-qubit gates must be better than the physical one-qubit gates in order for the logical qubit to have better error rates [5]. This is a very high bar to clear, especially for trapped-ion architectures which display extremely high single-qubit gate fidelities [10–12]. However, understanding how logical qubit gates perform in these systems is still necessary for EFTQC.

Current experimental demonstrations of quantum error correction have focused on generating the first individual logical qubits [5–8]. In such cases one need only compare against a discrete set of gates on the physical and logical qubit. From the perspective of applications, a more natural comparison is to ask when an EFTQC could outperform a NISQ device? In this case the NISQ device will use continuous single-qubit gates, whereas the EFTQC device must use a discrete gate set, implying extra circuit depth is needed to sequence continuous rotations over this discrete gate set. This implies that the EFTQC error rate must in fact be lower than the NISQ error rate to achieve the same precision of single-qubit gate operations.

In other words, the need to sequence continuous gates into discrete gates contributes to QEC overhead which EFTQC machines must overcome to outperform NISQ devices. Furthermore, long gate sequences realizing continuous rotations can compound coherent errors which QEC reduces but does not correct. Can error mitigation techniques such as randomized compiling help mitigate both the sequencing overhead and coherent errors on EFTQC devices?

---

\* Present address: Oak Ridge National Laboratory, Oak Ridge, TN 37830, USA

† Present address: HRL

In the present paper we examine the overhead of compilation into a discrete gate set and the efficacy of randomization over an ensemble of such compilations on Sandia National Laboratories’ QSCOUT trapped-ion device. This foreshadows future benchmarking efforts on EFTQC devices and provides a baseline for such benchmarks.

It should be emphasized that compilation and randomization of single-qubit rotations cannot possibly outperform the native physical continuous rotations on the NISQ device. However, the low errors of the single-qubit gates make accurate compiled realizations of continuous rotations possible. We are therefore able to make meaningful comparisons of randomized and unrandomized sequences. Because compilation is necessary on EFTQC devices this comparison tests a useful randomization technique for future calculations. In effect we are using the low noise single-qubit gates on ion traps as a resource for randomization.

This work is built upon the Solovay-Kitaev (SK) Theorem, which shows that it is possible to find efficient decompositions of continuous rotations into a discrete gate set [13–17]. This process is called *gate synthesis*, and is the focus of ongoing research [18–20].

Some gate synthesis algorithms attempt to calculate decompositions according to a cost metric, but do not try to perform exact synthesis to find the *most accurate* decomposition [16, 19, 21, 22]. That is, the user chooses some allowed precision  $\epsilon$ , and the algorithm finds a decomposition that approximates the desired rotation within that precision, according to some distance measure. These algorithms usually minimize the required number of  $T$ -gates.

This allowed precision  $\epsilon$  creates a degeneracy in the choice of decomposition, as there are many sequences  $R_i$  that achieve the same precision. Imposing a limit on the number of gates or number of  $T$  gates reduces the size of this ensemble of approximate rotations, but still allows for multiple different approximations of the same rotation of the same quality.

Previous works [19, 23, 24] focused on minimizing approximation error incurred during gate synthesis using probabilistic methods. Probabilistic state synthesis uses a weighted mixture of an ensemble of circuits to generate an approximation to a desired quantum state. The mixture over the ensemble results in better average accuracy than any individual circuit. Probabilistic state synthesis is therefore the state equivalent of randomized compilation (RC) [25], except the error to be minimized includes the synthesis error and not only the hardware error. This is the same notion that underlies *Multi-Product Formulas* [26] in Hamiltonian simulation.

Randomized Compilation is a technique that has been used in the NISQ era [27–29] to tailor coherent quantum errors into stochastic errors. The idea of randomized compilation is simple. A logical quantum circuit is duplicated  $r$  times, each copy being decomposed into a different random set of operations at the gate level.

Given a total sampling budget  $N$ , each of these circuits are then run on the device  $N/r$  times, and the resulting measurement outcomes are averaged together. This procedure maintains the global circuit structure but randomizes the gate sequence to mitigate the effects of coherent errors. Namely, RC via Pauli twirling can tailor coherent error into a Pauli channel, and RC via Clifford twirling can further tailor that error into a purely depolarizing channel.

In this work, we explore the effects of realistic quantum noise in addition to synthesis error when using SK sequences. We find that by using the degeneracy in sequence decomposition, we can make our rotations more robust to coherent errors by implementing a form of randomized compilation. We note that some sources of coherent noise can be corrected or at least mitigated by error correction codes intended for use with Solovay-Kitaev decompositions [30, 31]. However, the use of error correcting codes does not rule out coherent errors that can occur in error-corrected devices that merely suppress the error rather than eliminating it entirely. We will not discuss the physical origin of such errors here, but their existence is detrimental to error-corrected rotations.

This paper is structured as follows. We begin in Section II by detailing the algorithm that we use to generate SK sequences and analyzing the resulting ensemble of rotations. We then discuss the coherent noise model we use in Section III. In Section IV, we show results from a noiseless simulation of the technique, simulation under our simple coherent noise model, and experiment on a NISQ trapped-ion quantum computer. Finally, we summarize our findings in Section V.

## II. SEQUENCE ENSEMBLE

Before we present our results, we first discuss our method for generating distinct SK sequences. We then analyze the characteristics of the resulting ensemble and present our randomization algorithm.

### A. Generating Sequences

We consider decompositions into the set of  $\{H, S, T\}$  gates, as defined in equation (1):

$$H = \frac{1}{\sqrt{2}} \begin{bmatrix} 1 & 1 \\ 1 & -1 \end{bmatrix}, \quad S = \begin{bmatrix} 1 & 0 \\ 0 & i \end{bmatrix}, \quad T = \begin{bmatrix} 1 & 0 \\ 0 & e^{i\pi/4} \end{bmatrix} \quad (1)$$

These gates are sufficient to approximate any continuous one-qubit rotation about the  $X$ ,  $Y$ , or  $Z$  axes of the Bloch sphere, and are a common choice of gate-set. We will refer to a particular decomposition of a rotation as an *SK sequence*,  $R_i$ :

$$R_i = HST\dots ST \quad (2)$$

where  $i$  indexes the particular decomposition. These sequences or decompositions can approximate any rotation

$R(\hat{n}, \theta)$  about the axis  $\hat{n}$  by an angle  $\theta$ . It is sufficient to synthesize continuous rotations about one axis, because rotations about any axis can be synthesized from the gate set  $\{H, S, T\}$  and continuous rotations around one axis. We focus on approximating the  $R_Z(\theta)$  rotation.

The algorithm we use to generate our SK sequences is known as *gridsynth* [22]. It decomposes  $R_Z(\theta)$  rotations into the  $\{H, S, T\}$  gateset, minimizing the number of  $T$ -gates.  $T$ -gates are usually the most expensive gate due to the cost of magic state distillation [32–34]. The *gridsynth* algorithm is able to obtain solutions with  $T$ -counts  $t + \mathcal{O}(\log(\log(1/\epsilon)))$ , where  $t$  is the  $T$ -count of the second most optimal solution. We refer the reader to [22] for more details, but we do note a few aspects of interest.

The *gridsynth* algorithm takes as input a random seed, the desired rotation angle  $\theta$ , the binary precision  $\epsilon = 2^{-b}$  in realizing that rotation, and an “effort” integer to determine how much time the algorithm should spend finding an optimal solution. We may vary these parameters in order to generate multiple unique sequences for the same rotation. By varying the desired rotation angle  $\theta$  by a value smaller than  $\epsilon$ , we can find multiple different sequences that satisfy our precision constraint. These sequences may have slight variations in  $T$ -counts but are close enough to be grouped together in an equivalent ensemble. The gate count and  $T$ -count for these sequences increase linearly as a function of binary precision  $b$ , as can be seen in Figure 1.

We note that in order for a precision of  $\epsilon = 2^{-b}$  to affect the results of an experiment implementing a single rotation, it is necessary to also have an sufficient sampling budget. This requires a number of samples:

$$n \sim \mathcal{O}(\epsilon^{-2}) = 4^b \quad (3)$$

which grows very quickly with the desired precision. This shows that for any fixed number of samples there is an implied maximum value  $b_{\max}$  of  $b$  beyond which further increases in sequence precision are not distinguishable from sequences obtained with precision  $b_{\max}$ . Further discussion of sampling noise can be found at the end of Section IV A.

## B. SKARC Algorithm

In this subsection we outline our randomization procedure *Solovay Kitaev and Randomized Compilation* (SKARC) for a given quantum circuit  $C$  containing  $g$  different  $R_Z$  gates that rotate by unique angles and a total sampling budget  $N$ .

For each instance of an  $R_Z$  gate we wish to compile in  $C$ , we generate an ensemble of unique gate sequences  $R_i$ ,  $i = 1, 2, \dots, r$  by *gridsynth* as described in the Section II. These sequences can then be randomly selected with or without replacement in place of each corresponding  $R_Z$  rotation in  $C$ , with each combination of these selections resulting in a unique circuit  $C_j$ , where

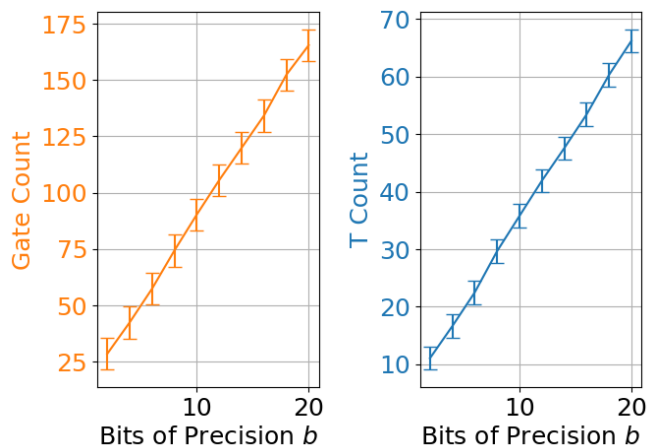


FIG. 1. Average gate count (left) and average  $T$ -gate count (right) for sequences generated by *gridsynth* as a function of the bits of precision  $b$ , where  $\epsilon = 2^{-b}$ . Error bars are the standard deviation over an ensemble of 100 sequences.

$j = 1, 2, \dots, r^g$  indexes the randomized circuit. It is possible to randomize over all  $r^g$  possible circuits, but usually unnecessary to see the benefits of randomization, so oftentimes the total number of randomized circuits can be truncated, as will be explored in this work in Section IV A. Once all circuits have been compiled this way, each circuit  $C_j$  is measured  $N/r^g$  times. The resulting  $N$  measurement outcomes are then combined into one distribution for analysis, effectively averaging the measurement results over  $r$  different decompositions of each  $R_Z$  gate.

For the purposes of this work, our circuit  $C$  is minimal, consisting of a single  $R_Z$  gate. We create and execute circuits for each SK sequence  $R_i$  where  $i = 0, 1, \dots, r$  and then measure each of these circuits in the  $X$ ,  $Y$ , and  $Z$  bases to perform state tomography. This results in  $3r$  different sets of measurement outcomes that can be used to reconstruct  $r$  Bloch vectors  $\vec{s}_i$ , one for each sequence:

$$\vec{s}_i = \langle X \rangle \hat{i} + \langle Y \rangle \hat{j} + \langle Z \rangle \hat{k} \quad (4)$$

An ensemble of  $m$  such vectors determine an average vector. This can be done either by combining the measurement results from each sequence together and calculating a new Bloch vector as described above, or by simply taking the average of the vectors obtained from each sequence. We define this mean vector for a particular choice of  $m$  sequences indexed by  $\{i_1, i_2, \dots, i_m\}$  as:

$$\vec{s}_{\{i_1, i_2, \dots, i_m\}} = \frac{1}{m} (\vec{s}_{i_1} + \vec{s}_{i_2} + \dots + \vec{s}_{i_m}) \quad (5)$$

If SKARC succeeds in mitigating error, then  $D(\vec{R}_Z, \vec{s}) < D(\vec{R}_Z, \vec{s}_i)$ , where  $\vec{R}_Z$  is the vector corresponding to the target  $R_Z$  rotation,  $\vec{s}$  is the mean vector for the entire ensemble, and  $\vec{s}_i$  is the vector for a single sequence chosen at random or optimized for its cost.

In order to quantify the performance of SKARC, we consider the trace distance between the target quantum

state and the mean quantum state from averaging. As these decompositions are for single-qubit rotations, the trace distance  $D(\vec{r}, \vec{s})$  is equivalent to half the Euclidean distance between the vectors on the Bloch sphere, where:

$$D(\vec{r}, \vec{s}) = \frac{|\vec{r} - \vec{s}|}{2} \quad (6)$$

A smaller trace distance indicates that we have better realized the target rotation.

Generating an ensemble of  $r$  sequences is the first step in employing averaging over sequences. We will use noiseless simulations to evaluate the effect of randomization on the accuracy of the results, as in [19, 23, 24]. In simulations with coherent noise added, and in experiment, we are evaluating the effect of randomization as a form of randomized compilation to mitigate coherent noise.

Across the ensemble of  $r$  total sequences generated by gridsynth, some of them are going to be more robust to certain types of noise than others. We can evaluate the variation between different ensembles of size  $m < r$  by sampling subsets of our overall ensemble of size  $m$ . It is intractable to consider all possible combinations for  $r = 100$  unique sequences, so instead we randomly choose at most  $q = 1000$  different ensembles of size  $1 \leq m \leq 100$  for simulation and  $1 \leq m \leq 20$  for experiment. We sample these sub-ensembles randomly with replacement and calculate the mean trace distance as:

$$D(m) = \frac{1}{q} \sum_{j=0}^q D(\vec{s}_{\{i_1, i_2, \dots, i_m\}_j}, \vec{R}_Z) \quad (7)$$

where  $\vec{R}_Z$  is the Bloch vector resulting from a noiseless, continuous  $R_Z$  rotation.

This average trace distance across 1000 possible combinations of sequences for a given ensemble size is then used to determine the efficacy of SKARC. In Section IV, we compare the average error with and without randomization as a function of the size of the ensemble that we average over. We should expect that as the size of the ensemble of distinct sequences increases, our error metrics will converge to some finite value. Moreover, by studying the characteristics of the ensemble of rotations implemented by our ensemble of circuits, we can learn more about the limits of SKARC.

### III. COHERENT NOISE MODEL

The coherent noise model we use in the remainder of this work is to multiplicatively over-rotate each rotation comprising a  $H$  gate in our circuit by a fraction  $1 + \delta$ , for some error strength  $\delta$ . This gate-dependent coherent noise model is similar to those used in [35, 36], and the original RC study [25], though the latter uses an additive over-rotation error rather than a multiplicative one. We only model simple, single-qubit coherent errors, as this work is focused only on single-qubit rotations. We only include  $H$  gates because on the QSCOUT ion trap the  $S$

and  $T$  gates are implemented with virtual  $R_Z$  rotations, and incur no error. The  $H$  gates are implemented as a product of gates  $X\sqrt{Y}$  and each of these gates is over rotated by  $\delta$  so that  $X(\delta) = R_x(\pi(1 + \delta))$  and  $\sqrt{Y(\delta)} = R_y(\frac{\pi}{2}(1 + \delta))$ .

We choose values of  $\delta$  that vary between  $[0, 10^{-2}]$ . If  $\delta$  were much larger than this, then it would be very difficult to resolve the desired  $\epsilon$ , even for a small number of bits of precision. On a real quantum device, the strength of this coherent over-rotation will depend on the error rate of the device in question and how much error correcting codes suppress errors.

The effect of this noise model on an individual SK sequence can be modeled as an erroneous single-qubit rotation. That is, if the noiseless approximate rotation is  $R_i(\hat{a}, \theta)$ , then the noisy rotation will be  $\tilde{R}_i = R_i\mathcal{E}$ . Where  $\mathcal{E} = R(\hat{b}, \phi)$  is a rotation of the state away from the noiseless result about an axis  $\hat{b}$  by an angle  $\phi$ . The axis and angle of this error will themselves be functions of the original axis  $\hat{a}$ , the original angle  $\theta$ , and the strength of the noise model  $\delta$ . However, the functional form of this error in terms of these parameters is non-trivial and sequence dependent. As a result, each sequence will experience this noise model in a unique manner. Averaging over many sequences will result in an ensemble of outputs converting the coherent noise to stochastic noise.

## IV. RESULTS

In this section, we present the results from two different wavefunction simulations using Sandia National Laboratories' JaqalPaq emulator [37], as well as an experiment on the QSCOUT device at Sandia National Laboratories [10], a trapped-ion NISQ computer. Noiseless simulation results are discussed in Subsection IV A. Results of simulations including the coherent noise model defined in Section III are discussed in Subsection IV B. Experimental results are discussed in Subsection IV C. Each of these sections will reference and compare data shown in Figures 2, 3, 4, and 5 which we will first describe here.

The simulated data comes from wavefunction simulations of the circuits that are equivalent to an infinite number of samples. In total,  $r = 100$  unique sequences were executed in simulation. The experimental data on the QSCOUT device was obtained from 24000 samples per measurement basis, and executed  $r = 20$  sequences. The circuit is comprised of an  $H$  gate to prepare the  $|+\rangle$  state, followed by an  $R_Z(\theta = 1)$  rotation, followed by measurement. We choose the  $|+\rangle$  state as our input state, as it is perpendicular to the axis of rotation on the Bloch sphere.

To visualize the distribution of Bloch vectors originating from different sequences, we plot them on a 2D projection of the Bloch sphere in Figures 2 and 3. Figure 2 shows data for precision  $b = 4$  and Figure 3 shows data for precision  $b = 7$ . The Bloch vector corresponding to the target rotation  $R_Z(\theta = 1)$  is used as the normal vector for the 2D projection and is shown as a black dot in

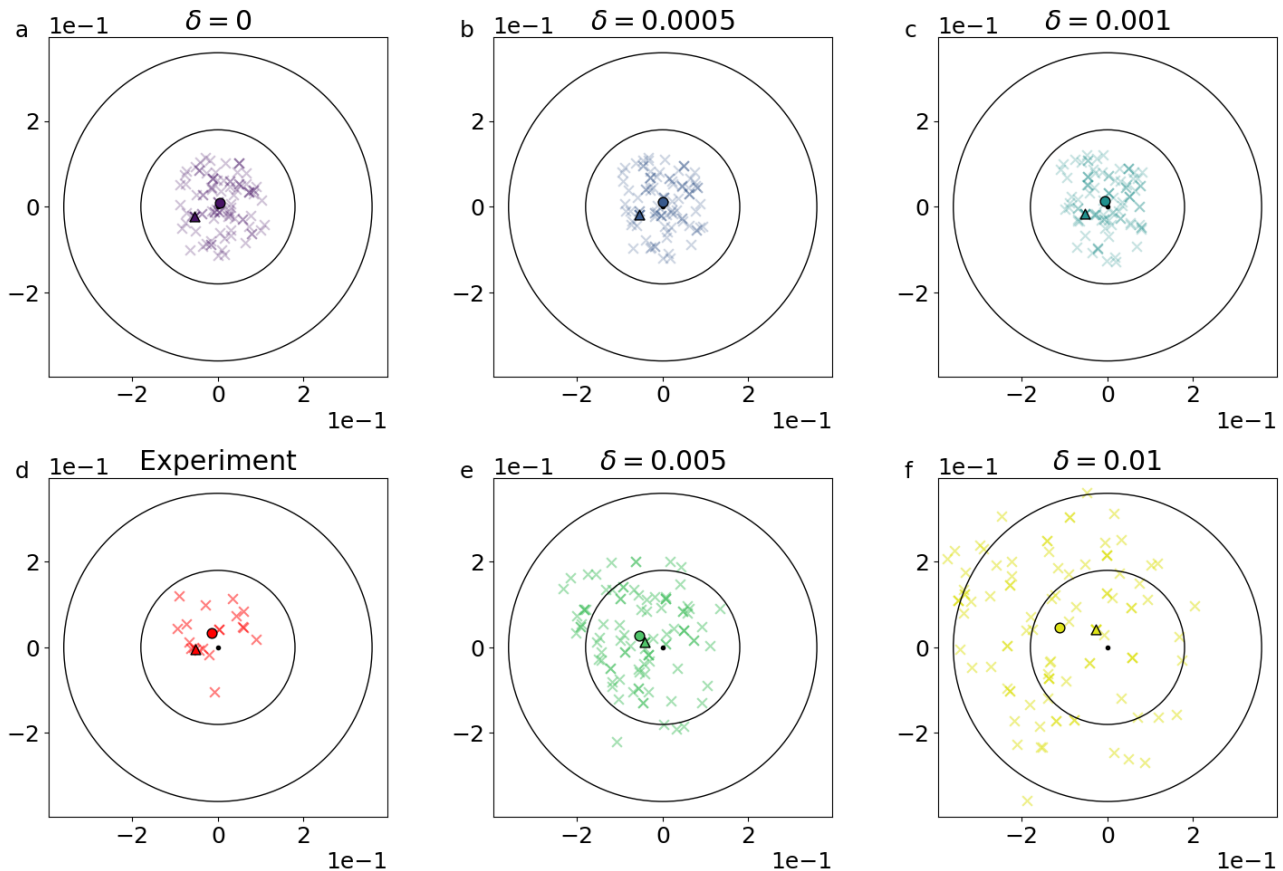


FIG. 2. Comparison of results from noiseless simulation, a coherent noise model, and experiment for precision  $b = 4$ . Plots are ordered left to right, top to bottom based on trace distance of the mean Bloch vector to the target rotation. **(a, b, c, e, f)** 2D projections of Bloch sphere vectors as a function of the strength of the coherent noise model  $\delta$ . Bloch vectors result from  $Z$ -rotations of the  $|+\rangle$  state relative to the noiseless, target  $R_Z$  rotation marked with a black circle in the center of the target. Vectors  $\vec{s}_i$  resulting from individual sequences are shown as crosses, and the vector corresponding to the sequence with fewest  $H$  gates is highlighted with a triangle. The mean of these vectors is shown as a circle. There is a bias in the vectors as a function of the noise, with larger  $\delta$  shifting left of center due to the cumulative effects of the coherent noise manifesting as a single biasing coherent rotation. **(d)** Projection of experimental data is shown in red, in the same manner as the simulated data. Only 20 sequences were measured for the experimental results, with each projective measurement using 24,000 shots. Trace distance for the mean Bloch vector falls between  $\delta = 0.001$  and  $\delta = 0.005$ .

the center of the target. The statevectors for each of the  $r$  SK sequences  $\vec{s}_i$  are shown as colored crosses, with the mean of these statevectors  $\vec{s}$  is shown as a circle. Experimental results are shown in red.

The triangle markers highlight the SK sequence with the smallest number of  $H$  gates, which is the least affected by noise in our noise model. For all precisions except  $b = 7$  and  $b = 10$ , the sequence with the fewest  $H$  gates is also the sequence with the fewest  $T$  gates, which is the normal output of the *gridsynth* algorithm. For precisions  $b = 7$  and  $b = 10$ , the sequence with the least  $H$  gates has the second-fewest  $T$  gates instead.

Figure 4 shows simulated and experimental trace distances as a function of the size of the ensemble of sequences  $m$  that we average over. The combinations of sequences are drawn randomly, with total number of possible combinations of sequences capped at 1000. For the simulated data, the precision of the sequences ranges

from  $b = [2, 20]$  in even increments from top to bottom. For the experimental data, the precision of the sequences ranges from  $b = [4, 5, 6, 7]$  from top to bottom for the solid lines. The dashed horizontal lines in the experimental data represent the trace distance for the optimal sequence with the fewest  $H$  gates and least expected error, colored in the same order as the mean trace distance data.

Figure 5 compares trace distances to the target rotation with and without SKARC for simulated and experimental data as a function of the bits of precision  $b$ . The solid lines with correspond to trace distances for mean Bloch vectors over the entire ensemble. The dashed lines correspond to trace distances for the optimal SK sequence. Here the error bars are calculated as the variance in the each of the  $X$ ,  $Y$ , and  $Z$  components of the Bloch vectors across the ensemble of sequences. This error is then propagated through to the trace distance calcula-

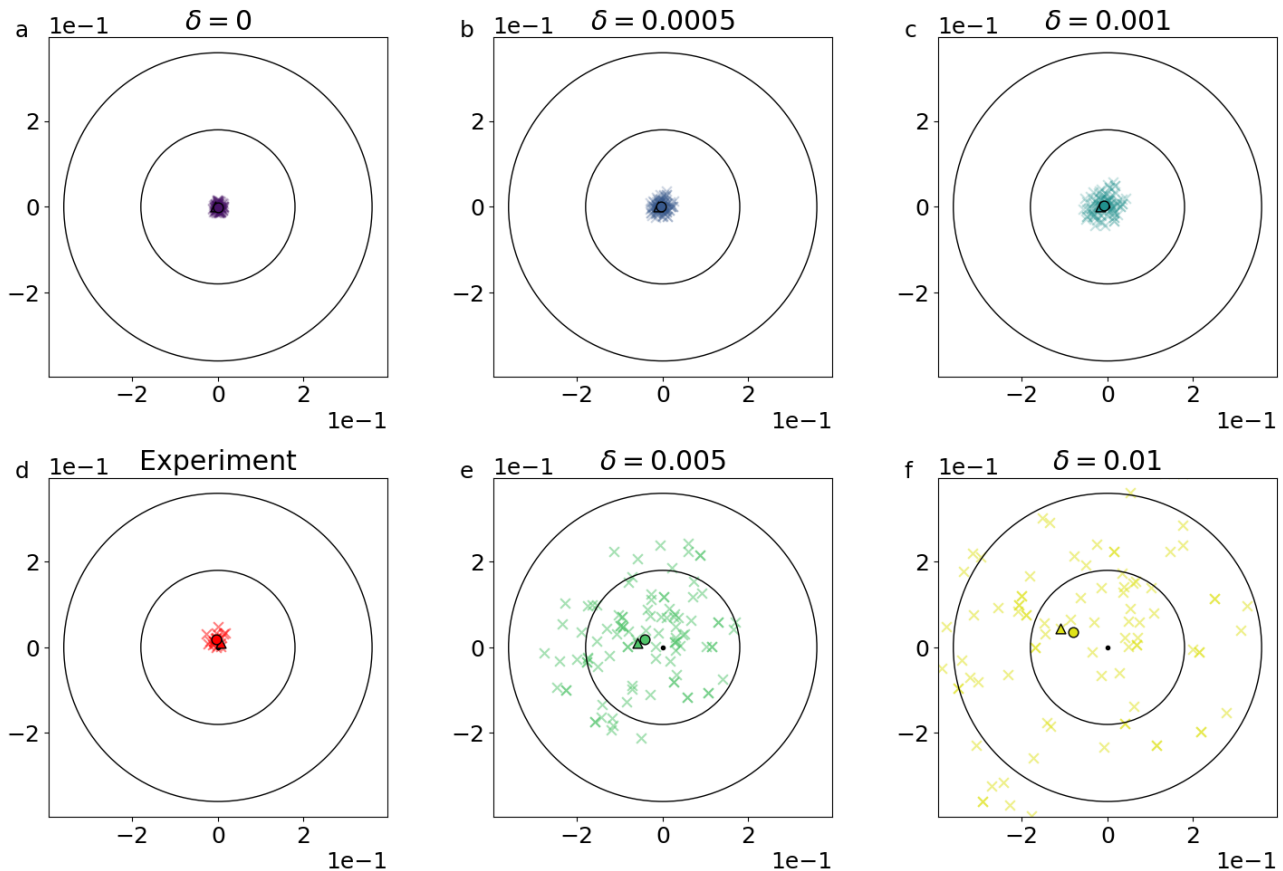


FIG. 3. Comparison of results from noiseless simulation, a coherent noise model, and experiment for precision  $b = 7$ . This data is collected and presented in the same manner as Figure 2. We note that the scale of the projection is the same in both figures. Increased precision shrinks the distribution of Bloch vectors in the absence of large coherent errors.

tion.

### A. Noiseless Simulation

We first consider the noiseless case of  $\delta = 0$ . Figures 2a, and 3a shows the distribution of Bloch vectors realized by the ensemble of SK sequences. As we increase the precision of the sequences from  $b = 4$  bits of precision to  $b = 7$ , we see that the vectors all cluster much closer to the target rotation as expected. The mean of the ensemble lies close to the target rotation in the center. This is the expected result, as the approximation error inherent to each individual sequence is randomly distributed, and thus will cancel out in aggregate. Moreover, this mean lies closer to the center than the optimal SK sequence highlighted with a triangle. This shows that use of randomization over SK sequences can improve the accuracy of the aggregate result.

The average trace distance as a function of the ensemble size  $m$  for a larger set of noiseless data for  $b = [2, 20]$  is shown in Figure 4a. We see that the mean trace distance decreases as the ensemble size increases, indicating that randomizing over more SK sequences leads to quantum

states that are closer to those of the target  $R_Z$  rotation. We note that taking into account the lowest value of the error bars in Figure 4a, the smallest possible trace distance would be achieved by averaging over less than the full circuit ensemble, which is expected. There will generally exist some particular combination of sequences that when averaged together will achieve a trace distance that is less than the trace distance for the average of the full ensemble. These sorts of algorithms are the basis of other probabilistic gate synthesis methods [19, 24]. That is, deliberately picking two sequences that are equally and oppositely spaced from the true rotation will give a very accurate result, but it requires more work to implement this sort of weighting of different unitaries.

The noiseless results in Figures 5a and b indicate that randomization improves accuracy. The trace distance for the mean Bloch vectors are about  $\simeq 0.15$  of the trace distances for the optimal Bloch vectors averaged over varying precisions. This improvement is consistent as the precision is increased, and is similar to increasing the bits of precision by 2 – 3. Using Figure 1, we see this is equivalent to a reduction of  $\sim 5 - 10$  in the required number of  $T$ -gates needed to achieve the desired precision, and a reduction in total gate count of  $\sim 15 - 25$ .



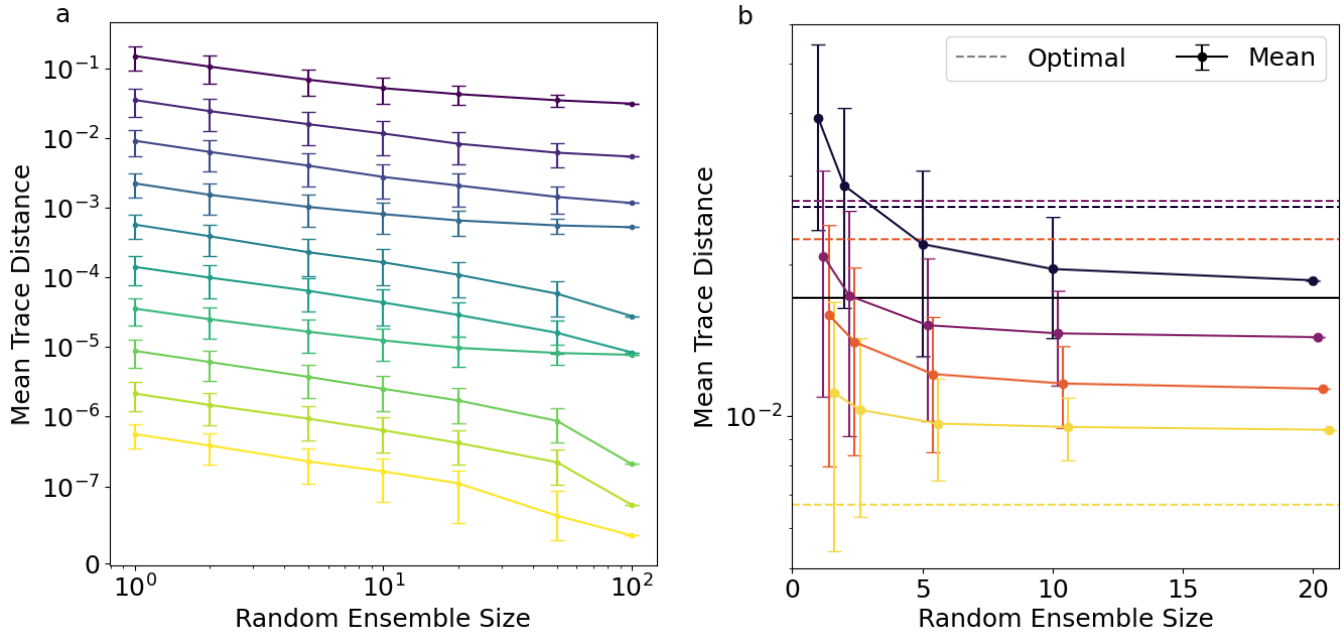


FIG. 4. **(a)** Simulation results of the mean trace distance across possible combinations of sequences for a given random ensemble size  $m \leq 100$ . Precision increases from  $b = [2, 20]$  in even increments from top to bottom. Only noiseless simulated data is shown. Accuracy increases with both precision and the size of the ensemble used for averaging. Error bars are taken as the standard deviation of the trace distances for all 1000 randomly chosen combinations of different sequences. **(b)** Experimental results of the mean trace distance. Precision increases from  $b = [4, 5, 6, 7]$  from top to bottom. Accuracy again increases with both precision and the size of the ensemble used for averaging. Error bars are calculated as for the simulated data, but for  $m \leq 20$ . Better accuracy can be obtained from choosing particular combinations of sequences as noted by the large error bars for smaller ensemble sizes. Trace distances for optimal sequences with fewest  $H$  gates are shown with dashed lines.

We also examined the relationship between the number of samples used in simulation and the accuracy of the rotation. For an approximation error of  $\epsilon = 2^{-b}$ , we would expect to need  $N = \epsilon^{-2} = 4^b$  samples to match. Using fewer samples than this means that imprecision due to sampling noise will overshadow any gains made by using more precise SK sequences. Using more samples than this means the opposite: that imprecision due to the approximation error of the sequence will overshadow any gains made by using more samples.

We see this trade-off in Figures 6a and 6b. The red line on these contour plots indicates the  $N = 4^b$  number of samples required for the theoretical best precision. We see that this lines up nicely with the shape of the contour itself. Improvements in precision (i.e. lower trace distance) can only be achieved by both increasing the number of samples and the precision of the sequence. This is also true for the randomized case. However, the randomized data generally show smaller trace distances than the non-randomized data, as expected. Using randomization, we can achieve better precisions without needing to increase the number of samples.

## B. Simulation with Coherent Noise

The question remains, do the improvements we see in the noiseless case hold in the presence of coherent noise? Single-qubit coherent errors manifest as unitary rotations on the Bloch sphere, and so in practice should be corrected in a manner similar to the synthesis error seen in the previous section. In order to answer this question, we repeat our analysis with the simple model of coherent noise described in Section III.

Figures 2 and 3b, c, e, and f, show that each individual sequence experiences the coherent error differently, as evidenced by the varied distributions of sequence vectors  $\vec{s}_i$  as a function of the coherent noise parameter  $\delta$ . However, the change is not totally random. The stronger the error strength, the more the ensemble shifts to the left, manifesting as a single coherent rotation on the surface of the Bloch sphere.

The performance of SKARC in the presence of coherent error is shown in Figure 5. The trace distance to the target rotation for simulation data falls with increasing bits of precision for nonzero  $\delta$  between  $b = 2$  and  $b = 7$ , before rising again for nonzero coherent noise. This shows that the noise has a limiting effect on the precision. Too much noise and it is impossible to realize highly precise rotations, regardless of whether averaging is used. This is

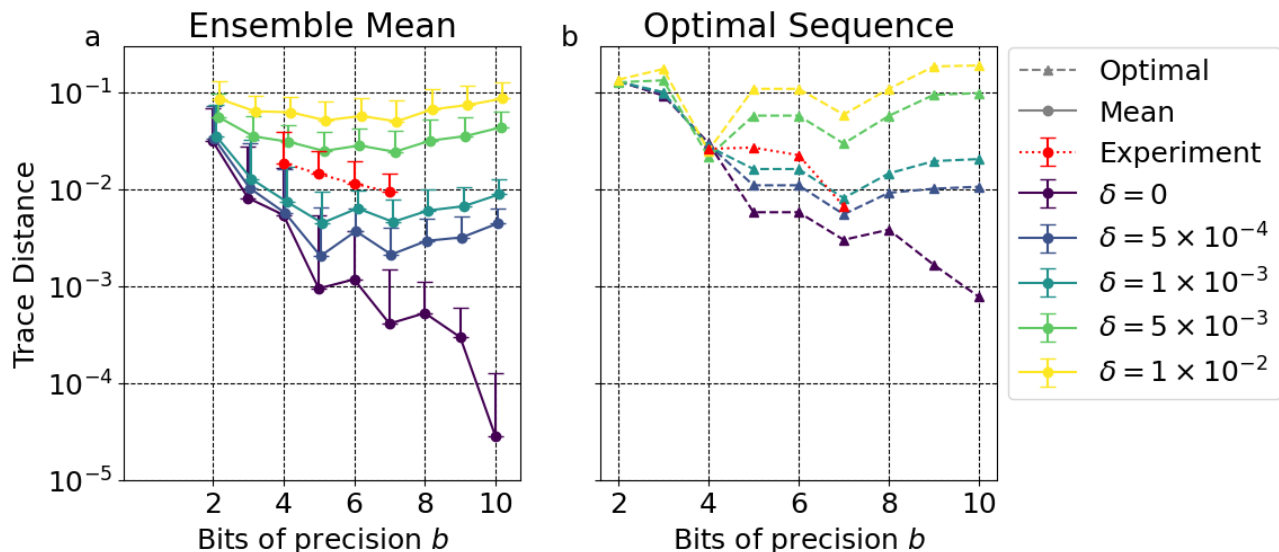


FIG. 5. Trace distance to the target rotation as a function of the bits of precision  $b$ . (a) Trace distance for the mean Bloch vector of the full ensemble of random sequences shown with solid lines and circles. The error bars are calculated from the variance in the components of the Bloch vectors across all sequences in the ensemble. Simulated data for different error strengths  $\delta$  are shown with circles. Experimental results are shown with red dotted lines and circles. (b) Trace distance for the sequence in the ensemble with the fewest  $H$  gates and least expected error shown with dashed lines and triangles. There are no error bars for this data, as there is only one sequence. Experimental results are shown with red dotted lines triangles.

again because the coherent error model shifts the overall distribution away from the target rotation.

Comparing the simulated data in Figure 5a and b, the trace distances for the mean Bloch vector are smaller than the trace distance of the sequence with the fewest  $H$  gates and least expected error. The exceptions are for precision  $b = 4$  and for some coherent noise strengths  $b = 7$ . We interpret this as the variability of the performance of the optimal sequence being larger than that of the mean, and therefore the optimal sequence sometimes outperforms the average.

### C. Experimental Results

We performed experiments on the QSCOUT device at Sandia National Laboratories [10], a trapped-ion NISQ computer. For this experiment, the gates are realized by using a microwave horn to apply pulses near-resonant with the 12.6428 Mhz separation of the qubit levels [10]. We used  $N = 24000 \sim 2^{14} \sim 4^7$  samples for each basis measurement due to time constraints, corresponding to a sampling error of  $\epsilon = 1/\sqrt{N} \sim 0.006$ . This means that for higher precisions than  $b = 7$ , finite sampling error dominates as opposed to the approximation error, as was discussed in Section IV A. As such, we restrict our experimental data to the range  $b = [4, 5, 6, 7]$ .

The Bloch vectors for each of the sequences  $R_i$  are shown in Figures 2d for  $b = 4$  and 3d for  $b = 7$  as red crosses, with the mean shown as a red circle. For precision  $b = 4$ , the spread of the experimental data is consistent with a value of  $\delta$  between  $1 \times 10^{-3}$  and  $\delta = 5 \times 10^{-3}$

in simulations. For precision  $b = 7$ , the spread of the experimental data is consistent with a value of  $\delta$  between  $1 \times 10^{-3}$  and  $\delta = 5 \times 10^{-3}$ . The Bloch vector corresponding to the sequence with the fewest  $H$  gates and least expected error is shown with a red triangle as part of the ensemble.

Figure 4b shows the trace distance of the mean of different ensemble sizes  $m$  across different bits of precision  $b$ . The trace distance decreases with higher precision and as the size of the random ensemble increases. The error bars in Figure 4b are calculated as the standard error on the mean of the distribution of trace distances for each possible combination of sequences for a given ensemble size. The trace distance for the optimal sequence with the fewest number of  $H$  gates is shown in 4b for comparison. For most precisions, this optimal sequence is further away than the mean sequence from averaging over the whole ensemble (the data points on the right). However, this is not the case for precision  $b = 7$ , where the optimal sequence is much more accurate than the average.

In Figure 5b we give the average trace distance for both simulations including coherent noise and for experiment. In Figure 5b, we compare the trace distance of the sequence with the fewest  $H$  gates. Again we find that the experimental data corresponds to an error rate of  $\delta \sim 2 \times 10^{-3}$ . We see larger trace distances for the optimal sequence when compared to averaging across different precision, though the experimental data point at  $b = 7$  is lower than expected, as was discussed previously. Moreover, this error rate is in agreement with, if slightly larger than the estimated error in single-qubit gates from other experimental benchmarks of the QSCOUT device



[10].

We see a reduction in the trace distance using SKARC to compute the mean vector compared to the sequence with the fewest  $H$  gates, except for the case of  $b = 7$ . Even in the presence of sampling noise and NISQ-era device noise, averaging the Bloch vectors of the ensemble renders a result that is closer to the target rotation, with improvement similar to that seen for the coherent noise model.

## V. CONCLUSIONS

We find that it is possible to reduce the effects of a wide variety of physical errors and approximation errors inherent to Solovay-Kitaev decompositions of continuous rotations by averaging over an ensemble of distinct gate sequences. Multiple similar-yet-distinct sequences are generated using the *gridsynth* algorithm by varying the target rotation as described in Section II A. When acting on a single-qubit quantum state, these sequences result in an ensemble of Bloch vectors that are clustered around the target rotation state as discussed in Section II B. By averaging the results of multiple circuits corresponding to each sequence, we are able to obtain quantum states that are closer to the ideal rotation as measured by the trace distance between the states.

We presented a noiseless simulation in Section IV A and analyze the ensemble of sequences that results. Across multiple desired approximation precisions  $\epsilon = 2^{-b}$  we find that the average of the full ensemble of sequences yields a Bloch vector that outperforms the sequence with the fewest  $H$  gates and least expected error. These results mirror those of other more sophisticated probabilistic gate synthesis algorithms such as convex hull finding [19, 24]. We study the effects of sampling noise on our method, and find the expected trend: The number of samples needed scales exponentially with the desired precision of the sequence, and under-sampling the circuit will lead to errors regardless of randomization. Similarly, over-sampling the circuit will be useless if the precision of the rotation is not increased in turn.

Improvement using randomization is maintained under a coherent noise model. In Section IV B we explore the effects of a simple multiplicative coherent noise model on the rotations comprising  $H$  gates in our circuit, mirroring performance on QSCOUT, a NISQ trapped-ion computer. Under such a model, SKARC can mitigate coherent errors and reduce the trace distance to the target rotation, though a coherent bias remains and limits the effectiveness of the method at realizing precise rotations with large coherent error.

Lastly, we study the technique on the QSCOUT device in Section IV C. We find that randomization can improve the accuracy of rotations on the device, though as with the coherent noise model, the resulting mean Bloch vector is still biased. The device performance is most closely replicated by a coherent error strength of  $\delta \sim 2 \times 10^{-3}$ ,

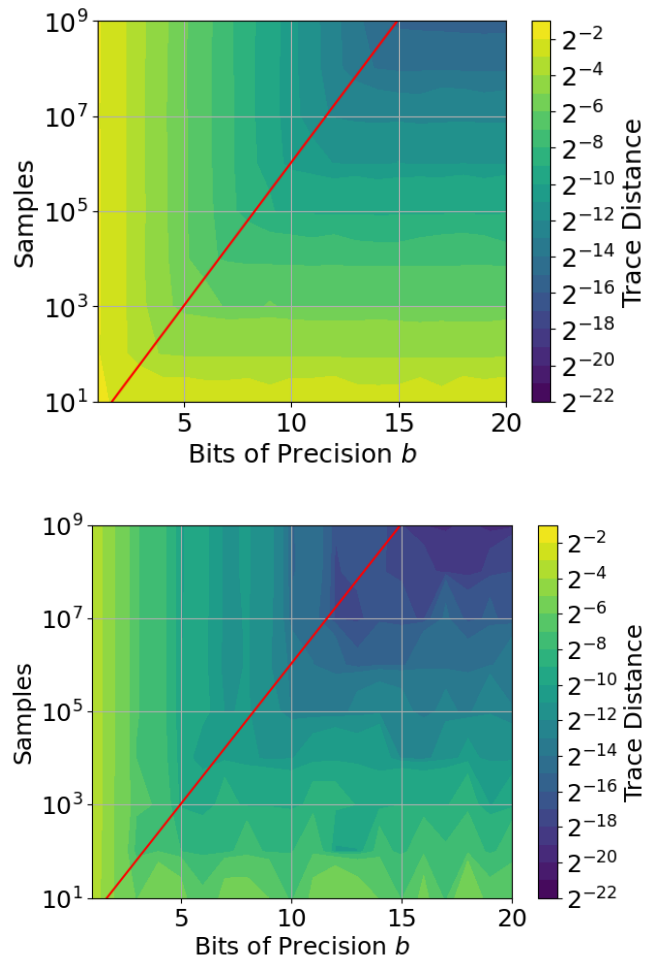


FIG. 6. Trace distance to an ideal  $R_Z$  rotation as a function of the number of samples and bits of precision. Results are shown without averaging over random sequences (top) and with randomization over the maximum ensemble size (bottom). The red line indicates the number of samples needed to match the approximation error  $\epsilon = 2^{-b}$  of an SK sequence. Using more samples above this line leads to diminishing returns in accuracy. Using a higher precision sequence with fewer samples to the right of this line also leads to diminishing returns.

or a 0.2% over-rotation, which matches with experimental benchmarks. Additionally, the number of samples required to realize high precision remains an obstacle in the near-term.

These results provide a NISQ baseline for single-qubit gate synthesis algorithms which we can compare against EFTQC devices in the future. Further research should be carried out for a wider variety of noise models that better capture the effects of error-correcting codes. Additionally, it would be of interest to benchmark all or a portion of this technique on an error-corrected qubit to see if the results hold under that paradigm. Methods such as SKARC that rest at the intersection of error mitigation and error correction will become more important as the EFTQC era approaches.

## VI. ACKNOWLEDGMENTS

This project was funded by the U.S. Department of Energy, Office of Science, Office of Advanced Scientific Computing Research Quantum Testbed Program. Sandia National Laboratories is a multi-mission laboratory managed and operated by National Technology and Engineering Solutions of Sandia, LLC, a wholly owned sub-

siary of Honeywell International Inc., for the U.S. Department of Energy’s National Nuclear Security Administration under contract DE-NA0003525. This paper describes objective technical results and analysis. Any subjective views or opinions that might be expressed in the paper do not necessarily represent the views of the U.S. Department of Energy or the United States Government. SAND2025-031500.

- 
- [1] John Preskill. Quantum computing in the nisq era and beyond. *Quantum*, 2:79, 2018.
- [2] Jonathan Wei Zhong Lau, Kian Hwee Lim, Harshank Shrotriya, and Leong Chuan Kwok. Nisq computing: where are we and where do we go? *AAPPS bulletin*, 32(1):27, 2022.
- [3] Zhenyu Cai, Ryan Babbush, Simon C Benjamin, Suguru Endo, William J Huggins, Ying Li, Jarrod R McClean, and Thomas E O’Brien. Quantum error mitigation. *Reviews of Modern Physics*, 95(4):045005, 2023.
- [4] Daniel A Lidar and Todd A Brun. *Quantum error correction*. Cambridge university press, 2013.
- [5] Laird Egan, Dripto M Debroy, Crystal Noel, Andrew Risinger, Daiwei Zhu, Debopriyo Biswas, Michael Newman, Muyuan Li, Kenneth R Brown, Marko Cetina, et al. Fault-tolerant control of an error-corrected qubit. *Nature*, 598(7880):281–286, 2021.
- [6] Suppressing quantum errors by scaling a surface code logical qubit. *Nature*, 614(7949):676–681, 2023.
- [7] Dolev Bluvstein, Simon J Evered, Alexandra A Geim, Sophie H Li, Hengyun Zhou, Tom Manovitz, Sepehr Ebadi, Madelyn Cain, Marcin Kalinowski, Dominik Hangleiter, et al. Logical quantum processor based on reconfigurable atom arrays. *Nature*, 626(7997):58–65, 2024.
- [8] Ivan Pogorelov, Friederike Butt, Lukas Postler, Christian D Marciniak, Philipp Schindler, Markus Müller, and Thomas Monz. Experimental fault-tolerant code switching. *Nature Physics*, pages 1–6, 2025.
- [9] Amara Katarawa, Katerina Gratsea, Athena Caesura, and Peter D Johnson. Early fault-tolerant quantum computing. *PRX Quantum*, 5(2):020101, 2024.
- [10] Susan M. Clark, Daniel Lobser, Melissa C. Revelle, Christopher G. Yale, David Bossert, Ashlyn D. Burch, Matthew N. Chow, Craig W. Hogle, Megan Ivory, Jessica Pehr, Bradley Salzbrenner, Daniel Stick, William Sweatt, Joshua M. Wilson, Edward Winrow, and Peter Maunz. Engineering the quantum scientific computing open user testbed. *IEEE Transactions on Quantum Engineering*, 2:1–32, 2021.
- [11] S. A. Moses, C. H. Baldwin, M. S. Allman, R. Ancona, L. Ascarrunz, C. Barnes, J. Bartolotta, B. Bjork, P. Blanchard, M. Bohn, J. G. Bohnet, N. C. Brown, N. Q. Burdick, W. C. Burton, S. L. Campbell, J. P. Campora, C. Carron, J. Chambers, J. W. Chan, Y. H. Chen, A. Chernoguzov, E. Chertkov, J. Colina, J. P. Curtis, R. Daniel, M. DeCross, D. Deen, C. Delaney, J. M. Dreiling, C. T. Ertsgaard, J. Esposito, B. Estey, M. Fabrikant, C. Figgatt, C. Foltz, M. Foss-Feig, D. Francois, J. P. Gaebler, T. M. Gatterman, C. N. Gilbreth, J. Giles, E. Glynn, A. Hall, A. M. Hankin, A. Hansen, D. Hayes, B. Higashi, I. M. Hoffman, B. Horning, J. J. Hout, R. Jacobs, J. Johansen, L. Jones, J. Karcz, T. Klein, P. Lauria, P. Lee, D. Liefer, S. T. Lu, D. Lucchetti, C. Lytle, A. Malm, M. Matheny, B. Mathewson, K. Mayer, D. B. Miller, M. Mills, B. Neyenhuis, L. Nugent, S. Olson, J. Parks, G. N. Price, Z. Price, M. Pugh, A. Ransford, A. P. Reed, C. Roman, M. Rowe, C. Ryan-Anderson, S. Sanders, J. Sedlacek, P. Shevchuk, P. Siegfried, T. Skripka, B. Spaun, R. T. Sprenkle, R. P. Stutz, M. Swallows, R. I. Tobey, A. Tran, T. Tran, E. Vogt, C. Volin, J. Walker, A. M. Zolot, and J. M. Pino. A race-track trapped-ion quantum processor. *Phys. Rev. X*, 13:041052, Dec 2023.
- [12] IonQ Staff. Ionq aria: Practical performance, Jan 2024. Accessed on Feb 29, 2024.
- [13] A Yu Kitaev. Quantum computations: algorithms and error correction. *Russian Mathematical Surveys*, 52(6):1191, Dec 1997.
- [14] Alexei Y. Kitaev. Quantum measurements and the abelian stabilizer problem. *Electron. Colloquium Comput. Complex.*, TR96(003), 1995.
- [15] A. Yu. Kitaev, A. H. Shen, and M. N. Vyalii. *Classical and Quantum Computation*. American Mathematical Society, USA, 2002.
- [16] Christopher M. Dawson and Michael A. Nielsen. The solovay-kitaev algorithm. *Quantum Info. Comput.*, 6(1):81–95, Jan 2006.
- [17] Michael A. Nielsen and Isaac L. Chuang. *Quantum Computation and Quantum Information: 10th Anniversary Edition*. Cambridge University Press, 2010.
- [18] Bálint Koczor. Sparse probabilistic synthesis of quantum operations. *PRX Quantum*, 5:040352, Dec 2024.
- [19] Seiseki Akibue, Go Kato, and Seiichiro Tani. Probabilistic unitary synthesis with optimal accuracy. *ACM Transactions on Quantum Computing*, 5(3), August 2024.
- [20] Nobuyuki Yoshioka, Seiseki Akibue, Hayata Morisaki, Kento Tsubouchi, and Yasunari Suzuki. Error crafting in mixed quantum gate synthesis. *arXiv: Quantum Physics*, 2025.
- [21] Ken Matsumoto and Kazuyuki Amano. Representation of quantum circuits with clifford and  $\pi/8$  gates. *arXiv: Quantum Physics*, 2008.
- [22] Neil J. Ross and Peter Selinger. Optimal ancilla-free clifford+t approximation of z-rotations. *Quantum Info. Comput.*, 16(11–12):901–953, September 2016.
- [23] Matthew B. Hastings. Turning gate synthesis errors into incoherent errors. *Quantum Inf. Comput.*, 17:488–494, 2016.
- [24] Earl Campbell. Shorter gate sequences for quantum computing by mixing unitaries. *Physical Review A*, 95(4),

- April 2017.
- [25] Joel J. Wallman and Joseph Emerson. Noise tailoring for scalable quantum computation via randomized compiling. *Phys. Rev. A*, 94:052325, Nov 2016.
- [26] Sergiy Zhuk, Niall F. Robertson, and Sergey Bravyi. Trotter error bounds and dynamic multi-product formulas for hamiltonian simulation. *Phys. Rev. Res.*, 6:033309, Sep 2024.
- [27] Matthew Ware, Guilhem Ribeill, Diego Ristè, Colm A. Ryan, Blake Johnson, and Marcus P. da Silva. Experimental pauli-frame randomization on a superconducting qubit. *Phys. Rev. A*, 103:042604, Apr 2021.
- [28] Akel Hashim, Ravi K. Naik, Alexis Morvan, Jean-Loup Ville, Bradley Mitchell, John Mark Kreikebaum, Marc Davis, Ethan Smith, Costin Iancu, Kevin P. O'Brien, Ian Hincks, Joel J. Wallman, Joseph Emerson, and Irfan Siddiqi. Randomized compiling for scalable quantum computing on a noisy superconducting quantum processor. *Phys. Rev. X*, 11:041039, Nov 2021.
- [29] Youngseok Kim, Andrew Eddins, Sajant Anand, Ken Xuan Wei, Ewout van den Berg, Sami Rosenblatt, Hasan Nayfeh, Yantao Wu, Michael Zaletel, Kristan Temme, and Abhinav Kandala. Evidence for the utility of quantum computing before fault tolerance. *Nature*, 618(7965):500–505, Jun 2023.
- [30] Daniel Greenbaum and Zachary Dutton. Modeling coherent errors in quantum error correction. *Quantum Science and Technology*, 3, 2016.
- [31] Sergey Bravyi, Matthias Englbrecht, Robert König, and Nolan Peard. Correcting coherent errors with surface codes. *npj Quantum Information*, 4, 2017.
- [32] E. Knill, R. Laflamme, and W. Zurek. Threshold accuracy for quantum computation. *arXiv: Quantum Physics*, 1996.
- [33] E. Knill, R. Laflamme, and W. Zurek. Resilient quantum computation: error models and thresholds. *Proceedings of the Royal Society A*, 454:365–384, Aug 1998.
- [34] Earl T. Campbell, Barbara M. Terhal, and Christophe Vuillot. Roads towards fault-tolerant universal quantum computation. *Nature*, 549(7671):172–179, Sep 2017.
- [35] Bichen Zhang, Swarnadeep Majumder, Pak Hong Leung, Stephen Crain, Ye Wang, Chao Fang, Dripto M. Debroy, Jungsang Kim, and Kenneth R. Brown. Hidden inverses: Coherent error cancellation at the circuit level. *Phys. Rev. Appl.*, 17:034074, Mar 2022.
- [36] Thorge Müller, Tobias Stollenwerk, David Headley, Michael Epping, and Frank K Wilhelm. Coherent and non-unitary errors in ZZ-generated gates. *Quantum Science and Technology*, 10(1):015058, dec 2024.
- [37] Andrew J. Landahl, Daniel S. Lobser, Benjamin C. A. Morrison, Kenneth M. Rudinger, Antonio E. Russo, Jay W. Van Der Wall, and Peter Maunz. Jaqal, the quantum assembly language for qscout. *arXiv: Quantum Physics*, 2020.